Available online at www.sciencedirect.com
SCIENCE DIRECT®
Journal of Computational Physics 199 (2004) 110–125
JOURNAL OF COMPUTATIONAL PHYSICS
www.elsevier.com/locate/jcp

Mesh stretch effects on convection in flow simulations

Tomoaki Ikeda [a], Paul A. Durbin [b,*]

[a] Department of Aeronautics and Astronautics, Stanford University, Stanford, CA 94305-3030, USA
[b] Department of Mechanical Engineering, Stanford University, Bldg 500, Stanford, CA 94305-3030, USA

Received 16 October 2003; received in revised form 3 February 2004; accepted 3 February 2004
Available online 10 March 2004

Abstract

Staggered grids have been widely used with finite difference approaches for incompressible flow simulation. They retain conservation properties that stabilize the flow field, and avoid odd–even decoupling in the pressure field. On a non-uniform mesh, however, the accuracy of finite difference schemes is degraded to the order of the mesh stretch, if all the conservation properties are to be upheld. This study shows how a non-uniform numerical mesh creates short wavelength errors in convective terms, especially when the grid spacing varies in the streamwise direction. The conservation properties of convective schemes on a non-uniform mesh can conflict with aspects of numerical accuracy. It is crucial to employ an area-weighted average for the convection velocity in order to impose mass conservation in the presence of mesh stretching. Truncation error analysis indicates that energy conserving schemes produce anti-diffusion error if the mesh is stretched, or positive diffusion if it is narrowed. An alternative convection scheme that minimizes the mesh-stretch error is proposed and evaluated through numerical simulations. The nature of mesh stretch error is illustrated by a direct numerical simulation of turbulent channel flow.

1. Introduction

As high-performance computer systems have become available, direct numerical simulation (DNS) of turbulent flow has been applied to increasingly complicated flow geometries. In many studies, the finite difference approach with a staggered grid system has been employed, with non-uniform mesh spacing near non-slip boundaries. With increasing geometrical complexity, stretching in the flow direction is sometimes unavoidable. This gives rise to some issues of numerical accuracy discussed herein.

In finite difference approximations, a numerical method that conserves mass, momentum, and kinetic energy has been preferred to obtain a numerically stable solution [1,4,5,7]. As physically unstable, complex fluid motions develop, the globally conserved quantities can stabilize numerics over the entire field, and ensure converged solutions. Morinishi et al. [6] showed that finite difference schemes (FDS) that conserve

* Corresponding author.
E-mail addresses: ikeda@cradle.co.jp (T. Ikeda), durbin@vk.stanford.edu (P.A. Durbin).

0021-9991/$ - see front matter © 2004 Elsevier Inc. All rights reserved.
doi:10.1016/j.jcp.2004.02.006

mass momentum and energy can be constructed using centered differences, to arbitrary order of accuracy, on a uniform, staggered grid system. Those schemes are referred to as *fully* conservative. The form of the convective terms may be *divergence*, *advective*, or *skew-symmetric*; they are all mathematically equivalent if the divergence-free condition is satisfied at the given order of accuracy.

However, Morinishi et al. [6] also show that, with non-uniform mesh spacing, the fully conservative form does not retain the accuracy that is achieved on a uniform mesh. If accuracy is enforced using geometric interpolation, conservation must be sacrificed by discarding symmetric, centered difference forms, and adding interpolation weights. Even if the lowest-order truncation errors are eliminated, diffusion effects arise in higher-order truncation terms, which destroys exact energy conservation. Since this additional error is multiplied by the convective velocity, mesh stretch in the streamwise direction must be minimized to suppress adverse effects. In steady state problems, an intensive mesh stretch is often applied only in the direction perpendicular to the flow. However, in unsteady simulations of turbulent flow, it is no longer possible to fix the mesh to the flow direction throughout the simulations, especially in relatively complicated geometries. Vortices that cross the stretched mesh region can be affected by the added diffusion. This leads to numerical errors that persist in statistical samples.

In this study, mesh stretch effects relevant to direct simulation of turbulent flow are investigated, from the viewpoints of effective accuracy and conservation properties of numerical schemes. We consider the incompressible turbulent flow governed by the Navier–Stokes equations,

$$\frac{\partial U_j}{\partial t} + \frac{\partial (U_j U_k)}{\partial x_k} = -\frac{\partial P}{\partial x_j} + \nu \frac{\partial^2 U_j}{\partial x_k \partial x_k}, \tag{1}$$

$$\frac{\partial U_k}{\partial x_k} = 0, \tag{2}$$

where U_1, U_2, and U_3 (or U, V, and W) are velocities in the x_1 (streamwise), x_2 (normal), and x_3 (spanwise) directions (or x, y, and z), respectively, P is pressure, and ν is molecular viscosity. We focus only on second-order centered difference schemes in a rectangular, non-uniform, staggered grid system, with three-point stencils applied in each spatial direction. Although the convection term of Eq. (1) is written in its divergence form, FDS are formulated in either divergence or advective form. In fact, the higher-order schemes are more easily modified in their advective forms on a non-uniform mesh, if their original accuracy is to be retained [6].

In the numerical tests of the present study, a fractional step method [2] is employed to advance the numerical solution in time. Static, not adaptive, meshes, of the type used in turbulence simulation, are at issue. The spatial derivatives in the directions with mesh stretch are implicitly solved by a second-order Crank–Nicolson scheme to avoid a CFL restriction. When three-dimensional examples are considered as numerical experiments, an equally spaced grid is used in the spanwise direction; then, the derivatives in that homogeneous direction are solved by an explicit third-order Runge–Kutta scheme, combined with the implicit Crank–Nicolson scheme [8]. At each substep of the semi-implicit scheme, the momentum equations are advanced with pressure terms left unchanged, then projected onto a divergence-free field to satisfy the continuity of Eq. (2) through the pressure correction function that obeys a Poisson equation.

2. Linear analysis

First we conduct a linear analysis to identify mesh stretch effects on a convection problem. On a uniform mesh, centered difference schemes only possess dispersive errors. However, diffusion effects arise with mesh stretching. Non-uniform mesh spacing can produce positive or negative diffusion. The wavelength dependence of diffusion errors will be investigated using Fourier series analysis. Fourier error analysis is

alternative to Taylor series analysis. The latter corresponds to the long wave limit. In turbulence simulation, errors at shorter wavelength inevitably are important.

2.1. Finite difference operators for linear problems

A simple analysis illustrates the effect of mesh stretch. We consider a linear wave equation with a constant convection velocity:

$$\frac{\partial u(x,t)}{\partial t} + c\frac{\partial u(x,t)}{\partial x} = 0. \tag{3}$$

With a three-point stencil at $j-1$, j, and $j+1$, the spatial derivative at x_j can be approximated as

$$\left.\frac{\partial u}{\partial x}\right|_j \approx C_j^+ \left.\frac{\delta u}{\delta x}\right|_{j+\frac{1}{2}} + C_j^- \left.\frac{\delta u}{\delta x}\right|_{j-\frac{1}{2}}, \tag{4}$$

where C_j^+ and C_j^- are constants to be provided. Note that Eq. (4) reads as an interpolation to x_j using the values at $x_{j+\frac{1}{2}}$ and $x_{j-\frac{1}{2}}$ with the weights C_j^+ and C_j^-.

In analogy to the convective schemes that will be introduced in Section 3.3, we examine the following three finite difference forms, denoted FD-1, FD-2, and FD-3, respectively:

- FD-1 volume weighted average

$$\delta_x^{\text{FD-1}} u = \frac{\overline{\delta u}^{\text{V},x}}{\delta x}, \tag{5}$$

- FD-2 arithmetic mean

$$\delta_x^{\text{FD-2}} u = \frac{\overline{\delta u}^{\text{A},x}}{\delta x}, \tag{6}$$

- FD-3 linear interpolation

$$\delta_x^{\text{FD-3}} u = \frac{\overline{\delta u}^{\text{L},x}}{\delta x}, \tag{7}$$

where the interpolates of a quantity ϕ are defined as

$$\left.\overline{\phi}^{\text{V},x}\right|_j \equiv \frac{\Delta x_{j+\frac{1}{2}}\phi(x_{j+\frac{1}{2}}) + \Delta x_{j-\frac{1}{2}}\phi(x_{j-\frac{1}{2}})}{\Delta x_{j+\frac{1}{2}} + \Delta x_{j-\frac{1}{2}}}, \tag{8}$$

$$\left.\overline{\phi}^{\text{A},x}\right|_j \equiv \frac{\phi(x_{j+\frac{1}{2}}) + \phi(x_{j-\frac{1}{2}})}{2}, \tag{9}$$

$$\left.\overline{\phi}^{\text{L},x}\right|_j \equiv \frac{\Delta x_{j-\frac{1}{2}}\phi(x_{j+\frac{1}{2}}) + \Delta x_{j+\frac{1}{2}}\phi(x_{j-\frac{1}{2}})}{\Delta x_{j+\frac{1}{2}} + \Delta x_{j-\frac{1}{2}}}. \tag{10}$$

The mesh spacing at $j+\frac{1}{2}$ is defined as $\Delta x_{j+\frac{1}{2}} \equiv x_{j+1} - x_j$, and the superscripts V, A, and L indicate *volume-weighted average*, *arithmetic mean*, and *linear interpolation*, respectively.

The weights, C_j^+ and C_j^-, for each form are given by the coefficients of ϕ in (8)–(10). With a volume-weighted average, the spatial difference (4) of the three-point stencil at x_j simply becomes the difference

between x_{i+1} and x_{i-1} as in the uniform mesh case. For data stored at the grid vertices, it can be written as

$$\delta_x^{\text{FD-1}} u\big|_j = \frac{u(x_{j+1}) - u(x_{j-1})}{\Delta x_{j-\frac{1}{2}} + \Delta x_{j+\frac{1}{2}}}. \tag{11}$$

This FD-1 conserves the quadratic quantity, u^2, or kinetic energy. The other two forms, FD-2 and FD-3, can be connected with the volume-weighted average by adding a diffusion term that is multiplied by mesh stretch:

$$\delta_x^{\text{FD-2}} u = \delta_x^{\text{FD-1}} u - \frac{\delta(\Delta x)}{4} \cdot \frac{\delta}{\delta x}\left(\frac{\delta u}{\delta x}\right), \tag{12}$$

$$\delta_x^{\text{FD-3}} u = \delta_x^{\text{FD-1}} u - \frac{\delta(\Delta x)}{2} \cdot \frac{\delta}{\delta x}\left(\frac{\delta u}{\delta x}\right), \tag{13}$$

where $\delta(\Delta x)\big|_j = \Delta x_{j+\frac{1}{2}} - \Delta x_{j-\frac{1}{2}}$.

The second-order diffusion error produced by FD-2 and FD-3, with $c > 0$, serves as extra diffusion if the mesh is narrowed in the convective direction, or as anti-diffusion if it is stretched. Since this error term is magnified by c, generally we should avoid extensive mesh stretch in the streamwise direction. The numerical error generated by the non-uniform mesh will be amplified and transferred downstream by the convective velocity.

2.2. The modified wavenumber for non-uniform grid spacing

Fourier error analysis identifies diffusive and dispersive errors on a *uniform* mesh. It characterizes the dependence of FDS on the wavenumber. However, even with non-uniform mesh spacing, Fourier analysis still provides useful information on mode dependence of the mesh stretch error; especially the high-frequency error, which is difficult to clarify solely by Taylor series analysis [3]. In a turbulent flow simulation, eddies at Kolmogoroff length scales have the highest frequency, and mesh stretch can cause unexpected effects on statistical samples. We extend Fourier error analysis to a non-uniform grid system, and evaluate the diffusive errors in terms of the modified wave number.

A function with a period L can be expanded in a Fourier series, and evaluated at discrete locations:

$$u(x_j, t) = \sum_{n=-\infty}^{\infty} \breve{u}_n(t) \mathrm{e}^{\mathrm{i}\frac{2\pi n}{L} x_j}, \tag{14}$$

where $\breve{u}_n$ is a Fourier coefficient in x-space, and $2\pi n/L$ is defined as the wave number, k_n, hereafter. The infinite Fourier expansion of a continuous function converges uniformly over the period L. When the derivative of $u(x)$ is computed, we can apply the spatial derivative to each element of the Fourier series:

$$\left.\frac{\partial u}{\partial x}\right|_j = \sum_{n=-\infty}^{\infty} \breve{u}_n \mathrm{i} k_n \, \mathrm{e}^{\mathrm{i} k_n x_j}. \tag{15}$$

The extension of the concept of a 'modified wavenumber' to a non-uniform mesh can be accomplished using this general Fourier expansion. When discrete functions are combined to represent a finite difference, it can be decomposed into the same linear sum of Fourier modes, if the functions are smoothly and continuously interpolated – which assures the uniform convergence of the linear combination. Then, a finite difference form of a first-order spatial derivative can be written as

$$\left.\frac{\partial u}{\partial x}\right|_j \approx \sum_m a_m^{(j)} u_{j+m} = \sum_{n=-\infty}^{\infty} \left[\sum_m a_m^{(j)} \mathrm{e}^{\mathrm{i}k_n x_{j+m}}\right] \breve{u}_n, \tag{16}$$

where $a_m^{(j)}$ is a coefficient of the FDS at the jth grid point. Comparing the Fourier expansions of the exact spatial derivative to its finite difference approximation, Eqs. (15) and (16), respectively, the modified wavenumber k_n^* on a non-uniform mesh can be defined as follows:

$$\sum_m a_m^{(j)} \mathrm{e}^{\mathrm{i}k_n(x_{j+m}-x_j)} \equiv \mathrm{i}k_{nj}^*. \tag{17}$$

Note that Eq. (17) is defined locally at the jth point, since the modified wavenumber has dependence on j.

For centered difference schemes using a three-point stencil of Eq. (4), a modified wavenumber is given as

$$k_{nj}^* = -\mathrm{i}\left[C_j^+ \frac{\mathrm{e}^{\mathrm{i}\theta_{nj}^+} - 1}{\Delta x_{j+\frac{1}{2}}} - C_j^- \frac{\mathrm{e}^{-\mathrm{i}\theta_{nj}^-} - 1}{\Delta x_{j-\frac{1}{2}}}\right], \tag{18}$$

where $\theta_{nj}^+ \equiv k_n \Delta x_{j+\frac{1}{2}}$, $\theta_{nj}^- \equiv k_n \Delta x_{j-\frac{1}{2}}$. The real and imaginary parts of the modified wavenumber can be written as follows:

$$k_{nj\,\mathrm{Real}}^* = C_j^+ \frac{\sin\theta_{nj}^+}{\Delta x_{j+\frac{1}{2}}} + C_j^- \frac{\sin\theta_{nj}^-}{\Delta x_{j-\frac{1}{2}}}, \tag{19}$$

$$k_{nj\,\mathrm{Imag}}^* = -C_j^+ \frac{\cos\theta_{nj}^+ - 1}{\Delta x_{j+\frac{1}{2}}} + C_j^- \frac{\cos\theta_{nj}^- - 1}{\Delta x_{j-\frac{1}{2}}}. \tag{20}$$

Eq. (19) can be considered to be a linear average of $\sin(k\Delta x)/\Delta x$ at $j+\frac{1}{2}$ and $j-\frac{1}{2}$. Note that $\sin(k\Delta x)/\Delta x$ is the modified wavenumber of a three-point centered difference scheme on a uniform grid.

In the convection problem of Eq. (3), $k_{nj\,\mathrm{Real}}^*$ represents the oscillation of a mode. Then $k_{nj\,\mathrm{Imag}}^*$ either amplifies (if $ck_{nj\,\mathrm{Imag}}^* > 0$) or damps (if $ck_{nj\,\mathrm{Imag}}^* < 0$) its magnitude. In the case of a uniform grid with an anti-symmetric centered difference, $k_{nj\,\mathrm{Imag}}^*$ vanishes; only a dispersive error remains in the sense that $k_n^* \neq k_n$.

We are primarily interested in the imaginary part of the modified wavenumber, Eq. (20). For convenience, we define some geometric parameters,

$$\Delta x_j^{\mathrm{M}} \equiv (\Delta x_{j+\frac{1}{2}} + \Delta x_{j-\frac{1}{2}})/2$$

and

$$\epsilon_j \equiv (\Delta x_{j+\frac{1}{2}} - \Delta x_j^{\mathrm{M}})/\Delta x_j^{\mathrm{M}} = (\Delta x_j^{\mathrm{M}} - \Delta x_{j-\frac{1}{2}})/\Delta x_j^{\mathrm{M}}.$$

ϵ is defined as the mesh stretch normalized by local mesh spacing. Note $\Delta x_{j+\frac{1}{2}} = (1+\epsilon_j)\Delta x_j^{\mathrm{M}}$ and $\Delta x_{j-\frac{1}{2}} = (1-\epsilon_j)\Delta x_j^{\mathrm{M}}$.

Then, for the interpolations shown in Eqs. (5)–(7), the diffusive part of the wavenumbers are

$$k_{j\,\mathrm{Imag}}^{*\,\mathrm{FD\text{-}1}} = -\frac{1}{2\Delta x_j^{\mathrm{M}}}\left\{\cos\theta_j^+ - \cos\theta_j^-\right\}, \tag{21}$$

$$k_{j\,\mathrm{Imag}}^{*\,\mathrm{FD\text{-}2}} = -\frac{1}{2\Delta x_j^{\mathrm{M}}}\left\{\frac{1}{1+\epsilon_j}\left(\cos\theta_j^+ - 1\right) - \frac{1}{1-\epsilon_j}\left(\cos\theta_j^- - 1\right)\right\}, \tag{22}$$

$$k^{*\,\mathrm{FD\text{-}3}}_{j\,\mathrm{Imag}} = -\frac{1}{2\Delta x^{\mathrm{M}}_j}\left\{\frac{1-\epsilon_j}{1+\epsilon_j}\left(\cos\theta^{+}_j - 1\right) - \frac{1+\epsilon_j}{1-\epsilon_j}\left(\cos\theta^{-}_j - 1\right)\right\}, \tag{23}$$

where the index n was dropped. Assuming that c is positive, Eq. (17) is consistent with positive-diffusion if $k^{*}_{j\,\mathrm{Imag}} < 0$, or anti-diffusion if $k^{*}_{j\,\mathrm{Imag}} > 0$.

Fig. 1 shows the diffusive part of the modified wavenumbers versus $k\Delta x^{\mathrm{M}}$ at several values of ϵ, for the three forms of Eqs. (21)–(23). The modified wavenumber is multiplied by local mesh spacing Δx^{M}, and also divided by ϵ in the diagram.

A few comments: First, the diffusivity depends locally on $k\Delta x^{\mathrm{M}}$, rather than on a global Fourier wavenumber, k. Thus, one Fourier mode provides a variable diffusion error at different points of the mesh. Second, the sign of the mesh stretch ratio ϵ determines whether it shows positive- or negative-diffusion. Third, for the smaller values of ϵ, 0.2 and 0.01 in the diagram, the dependence on ϵ is insignificant in the normalized form $k^{*}_{\mathrm{Imag}}\Delta x^{\mathrm{M}}/2\epsilon$ that is plotted.

In the DNS cases of Section 4, ϵ is less than 0.1. Therefore, k^{*}_{Imag} depends approximately linearly on the non-dimensionalized mesh-stretch ratio,

$$2\epsilon_j = (\Delta x_{j+\frac{1}{2}} - \Delta x_{j-\frac{1}{2}})/\Delta x^{\mathrm{M}}_j.$$

This Fourier analysis of error might be justified by the following considerations. In a general Fourier expansion, all Fourier modes with $k_n \to \infty$ must be included, whereas simulation on a uniform grid requires only discrete wavenumbers up to $\pm\pi/\Delta x$. However, if a discrete function is replaced by a continuous, sufficiently smooth function, and if the lower-frequencies are dominant, a finite Fourier series up to the order $k_n\Delta x = \pi$ will be a good approximation of the exact function. Considering that the diffusive error shown in Eq. (20) depends on a local Fourier mode, sufficient smoothness can be assumed. Locally, the shortest wavelength is on the order of the mesh spacing; Fourier modes higher than this are insignificant if the grid resolution is not extremely coarse.

Among the three schemes examined here, FD-1 (Eq. (5)) exhibits an anti-diffusion error throughout $0 \leqslant k\Delta x^{\mathrm{M}} \leqslant \pi$ for positive ϵ, i.e., in a mesh-expanding region. For $\epsilon < 0$, it shows purely diffusive error within $0 \leqslant k\Delta x^{\mathrm{M}} \leqslant \pi$. This behavior corresponds to the usual second-order diffusion, which is the lowest-truncation error. At low wavenumbers, approximately up to $k\Delta x^{\mathrm{M}} \simeq 0.7\pi$, the magnitude of the modified wavenumbers is larger than those of the other two schemes. Beyond that, however, $|k^{*}_{\mathrm{Imag}}|$ decreases and reaches zero at $k\Delta x^{\mathrm{M}} = \pi$, due to higher-order errors, also caused by mesh stretching.

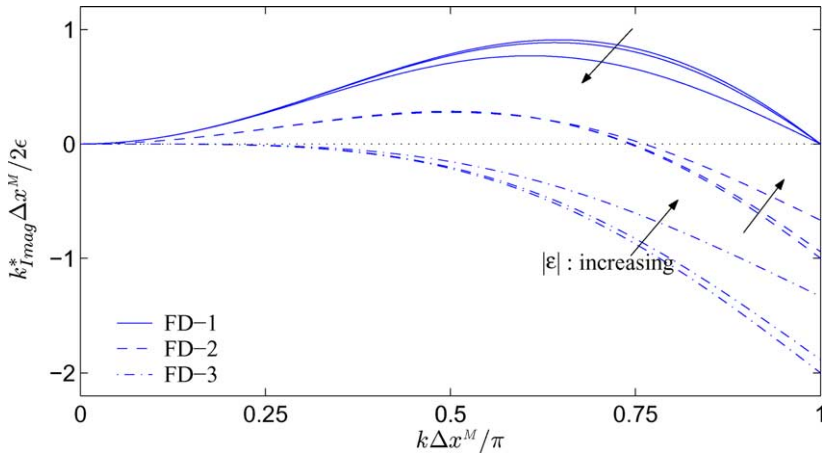

Fig. 1. Imaginary (diffusive) part of modified wavenumber diagrams of FDS for $\epsilon = \pm 0.01, 0.2, 0.5$.

Since FD-3 (Eq. (7)) eliminates the lowest-order mesh stretch error, the long wavelength diffusion that is observed in the other two schemes is removed, as shown in Fig. 1. However, the diffusive error of FD-3 increases at higher wavenumbers. As the wavenumber goes up to $\pi/\Delta x^{\mathrm{M}}$, it produces the largest diffusive error among these three forms. For negative ϵ, or in a mesh-narrowing region, it leads to an unstable mode. Hence, this scheme may affect the eddies of the smallest size, such as the Kolmogoroff length scale. Evidence of this adverse effect will be presented in Section 2.3.

As FD-2 (Eq. (6)) retains second-order diffusion with a reduced coefficient, positive- and anti-diffusions are mixed in higher- and lower-frequency regions. The FD-2 curve lies in the middle of FD-1 and FD-3 over a conventional range of Fourier modes.

2.3. Linear convection tests

The observations on the Fourier mode dependence can be verified in a numerical test. The linear convection problem represented by Eq. (3) was solved using the three forms of interest on a cell-centered stretched mesh, with inter-cell faces $x_{j+\frac{1}{2}} = \xi_j + \frac{1}{4\pi}\sin(2\pi\xi_j)$ for $0 \leqslant \xi \leqslant 1$, $\xi_j = j/N$ $(j = 0, 1, \ldots, N)$, with $N = 32$. The mesh is narrowed in $0 < x < 0.5$, and expanded in $0.5 < x < 1$. As initial conditions, low- and high-frequency modes in computational space, $u|_{t=0} = \cos(2\pi n_\xi \xi_j)$ with $n_\xi = 2$ and $N/2$, were prescribed. Here n_ξ signifies a Fourier mode in computational space. The finite-difference equation was advanced using the Crank–Nicholson scheme with a periodic boundary condition at the ends, $x = 0$ and 1. Crank–Nicholson was chosen because it is common in turbulence simulation. The linear tests were run for one period of time, so that the analytical solution coincides with the initial state.

Fig. 2 shows the case of a low-wavenumber mode. The solutions at the final state and its Fourier spectrum in computational space are presented. Because of low grid resolution, the solutions show considerable distortion from the initial profile for all the schemes. However, the higher-frequency error that appears in the mesh-stretching region, $x > 0.5$, shows the characteristic of each scheme. The volume-weighted average form produces the largest oscillations in the solution. Non-uniform grid spacing induces higher-frequency modes – which is illustrated in the Fourier mode diagram. The linear interpolation form shows the least amount of higher-frequency error. The arithmetic mean form produces slightly larger errors than the linear interpolation form in the high wavenumber region.

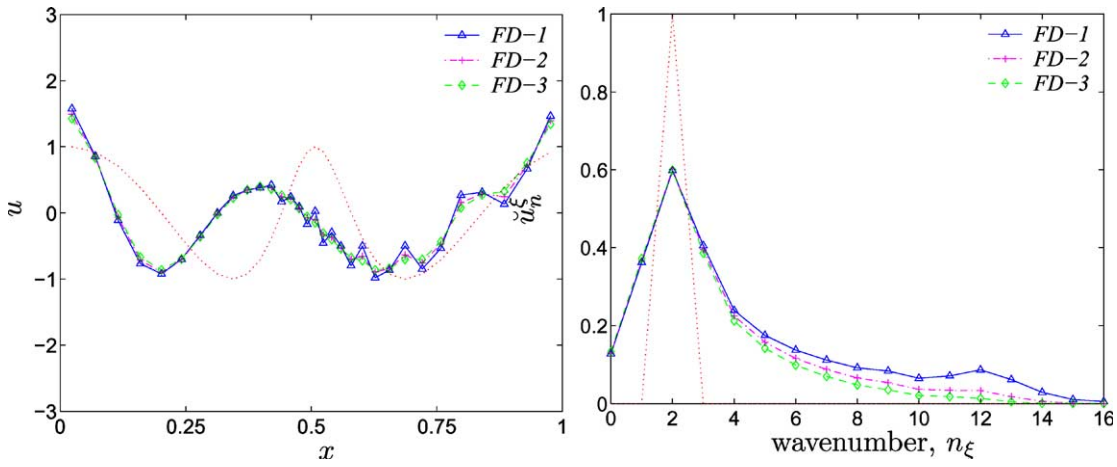

Fig. 2. Comparison between the three forms in a linear convection problem using a low-frequency wave ($n_\xi = 2$) as an initial state. Solutions after one period of time (*left*) and their Fourier modes in the computational ξ-space (*right*). Dotted line denotes the initial state, or analytical solution.

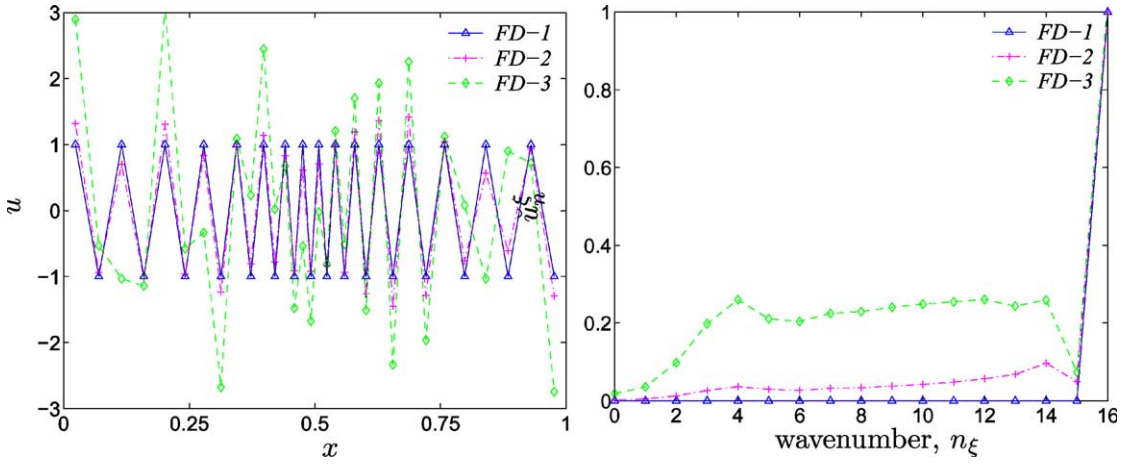

Fig. 3. Comparison between the three forms in a linear convection problem with a high-frequency wave ($n_\xi = N/2$) as an initial state. See the caption of Fig. 2.

The same tendency was observed not only in this linear convection problem, but also in a non-linear vortex convection test [3]. An adequately resolved vortex can be considered to be composed of relatively low-wavenumber modes. In this experiment, although not shown in the present paper, a two-dimensional Taylor vortex was convected by a uniform flow on a non-uniform mesh, which first narrowed then stretched in the streamwise direction. Scheme I of Section 3 showed the largest oscillation in the mesh stretching region, where the convective scheme produces anti-diffusion. This oscillatory behavior was minimized by Scheme III of Section 3 by removing the lowest-order truncation error.

Fig. 3 shows the case of a high-frequency initial condition. Since the highest-frequency mode is a stationary solution for the volume-weighted average form, no time advance occurs in the solution. As has been expected from Fig. 1, the linear interpolation form shows the largest deviation from the initial state. In its Fourier mode diagram, lower modes are excited over a wide range of wavenumbers, although the resulting highest-frequency mode does not change significantly from the initial state. These lower-frequency errors are significantly reduced in the arithmetic mean form, which is confirmed by both the physical and Fourier spaces in Fig. 3.

To summarize the above results, the volume-weighted average form adversely affects the lower-frequency waves, while the linear interpolation form, which shows the best performance in a low-frequency simulation, spoils a high-frequency wave to an excessive degree. The arithmetic mean form does not show the best result in either test; however, its mixed effects of positive and negative diffusions for lower and higher wavenumbers lead to acceptable performance for both the cases. The effects of these errors produced in lower- and high-frequency modes will be evaluated in a full Navier–Stokes simulation in Section 4.

3. The formulation of convective schemes

3.1. Conservation properties of FDS

We are concerned with the effects of mesh on computations of incompressible fluid flow, especially as relates to turbulence simulation. The development here is necessarily brief; see Ikeda and Durbin [3] for more details. As a preliminary, the conservative form of a FDS is reviewed.

In a time evolving process represented by the following partial differential equation

$$\frac{\partial \phi}{\partial t} + Q(\phi) = 0, \tag{24}$$

the term $Q(\phi)$ is *conservative* if it can be written in divergence form,

$$Q(\phi) = \nabla \cdot \vec{F}(\phi) = \frac{\partial F_x(\phi)}{\partial x} + \frac{\partial F_y(\phi)}{\partial y} + \frac{\partial F_z(\phi)}{\partial z}. \tag{25}$$

It is common practice to derive an integral form of conservation equation by integrating Eq. (24) over an arbitrary, time-independent, closed domain Ω and applying Gauss' theorem:

$$\frac{\mathrm{d}}{\mathrm{d}t}\int_{\Omega} \phi \,\mathrm{d}V + \int_{\partial\Omega} \vec{F}(\phi) \cdot \mathrm{d}\vec{S} = 0. \tag{26}$$

Eq. (26) shows that the net flux $\vec{F}$, crossing the surface $\partial\Omega$, causes the rate of change with time of the volume integral of ϕ over the domain Ω.

Eq. (26) is the basis for finite volume formulations. A numerical cell is regarded as the control volume Ω, and the net flux into the cell is balanced by the time difference of the function ϕ, which is defined as the average over the cell. Moreover, a finite difference formulation corresponding to Eq. (26) on a micro-scale is introduced by setting up a control volume for each node point in a vertex grid system. Conservation on a global-scale is shown by summing the function ϕ times volume weights over the entire region [2]. These ideas lead to a discretized conservation form, from a finite difference viewpoint.

We consider a structured, non-uniform Cartesian grid. Locations x_j and $x_{j+\frac{1}{2}}$ will be needed. The jth index is defined as a node point, and $j+\frac{1}{2}$ comes in the middle of two points, j and $j+1$. In a vertex grid system, variables are available at j; in a cell-centered grid system, they are at $j+\frac{1}{2}$ [2, chapter 4].

To see the conservation properties in a finite difference form, we define the discrete derivative operator for a non-uniform, rectangular mesh at the jth point in the x-direction as

$$\left.\frac{\delta f}{\delta x}\right|_j \equiv \frac{f(x_{j+\frac{1}{2}}) - f(x_{j-\frac{1}{2}})}{x_{j+\frac{1}{2}} - x_{j-\frac{1}{2}}}. \tag{27}$$

Instead of Eq. (27), we may also have to define the finite difference operator at $j+\frac{1}{2}$, not at j as shown. In this case, we only need to shift the indices by $\frac{1}{2}$. Using this operator, the term $Q(\phi)$ in Eq. (24) is *conservative* for the quantity ϕ when discretized with the second-order centered difference, if $Q(\phi)$ can be written as

$$Q(\phi) = \frac{\delta F_x(\phi)}{\delta x} + \frac{\delta F_y(\phi)}{\delta y} + \frac{\delta F_z(\phi)}{\delta z}. \tag{28}$$

This definition corresponds to Eq. (25), but in a discrete form, and is conservative if the numerical volume integration obeys a discrete Gauss theorem equivalent.

3.2. The numerical flux and interpolation operators

The formulation of numerical fluxes on a stretched mesh is considered here. Although only the two-dimensional formulation is presented for simplicity, the following argument can be applied to the three-dimensional case with no difficulty.

With the finite difference operator, the discrete continuity on a two-dimensional staggered grid is written as

$$\frac{\partial U}{\partial x} + \frac{\partial V}{\partial y} \approx (\mathrm{Cont.}) \equiv \frac{\delta U}{\delta x} + \frac{\delta V}{\delta y}. \tag{29}$$

In a staggered grid system, continuity is evaluated at each cell center, and the numerical flux of mass is provided at each cell face. Therefore, second-order accuracy is retained for mass conservation, even with mesh stretching.

In momentum equations, an equivalence between divergence and advective forms is analytically achieved if continuity is enforced. For example, the advective form for U-velocity can be connected with the divergence form as

$$U\frac{\partial U}{\partial x}+V\frac{\partial U}{\partial y}=\frac{\partial UU}{\partial x}+\frac{\partial UV}{\partial y}-U\cdot\left(\frac{\partial U}{\partial x}+\frac{\partial V}{\partial y}\right). \tag{30}$$

When a momentum equation is solved by a finite volume approach, fictitious cell-faces are set up for each velocity component [2, p. 73]. A resulting control volume is composed of two adjoining half cells, as shown in Fig. 4. Therefore, the mass conservation in the control volume must be evaluated as an average of the two cells.

To correctly represent the mass flux crossing the cell faces, we define the *area-weighted* average operator applied to a convective velocity component ϕ in the x-direction at an inter-cell location as (see Fig. 4)

$$\widehat{\phi}^{x}\Big|_{j+\frac{1}{2}}\equiv\frac{S^{\phi}_{j+1}\phi(x_{j+1})+S^{\phi}_{j}\phi(x_{j})}{S^{\phi}_{j+1}+S^{\phi}_{j}}, \tag{31}$$

where S^{ϕ} is the area of a cell face on which ϕ is defined in a staggered grid, e.g., $S^{U}=\Delta y\Delta z$, $S^{V}=\Delta x\Delta z$, and $S^{W}=\Delta x\Delta y$ in the three-dimensional case. With definition (31) mass flux is conserved by the continuity equation. Note that on a rectangular grid, $\widehat{U}^{x}=\overline{U}^{\mathrm{A},x}$, $\widehat{V}^{x}=\overline{V}^{\mathrm{V},x}$.

Interpolation operators are defined in Eqs. (8)–(10). We replace the first by

$$\overline{\phi}^{\mathrm{V},x}\Big|_{j}\equiv\frac{\Delta x_{j+\frac{1}{2}}\phi(x_{j+\frac{1}{2}})+\Delta x_{j-\frac{1}{2}}\phi(x_{j-\frac{1}{2}})}{2(x_{j+\frac{1}{2}}-x_{j-\frac{1}{2}})}, \tag{32}$$

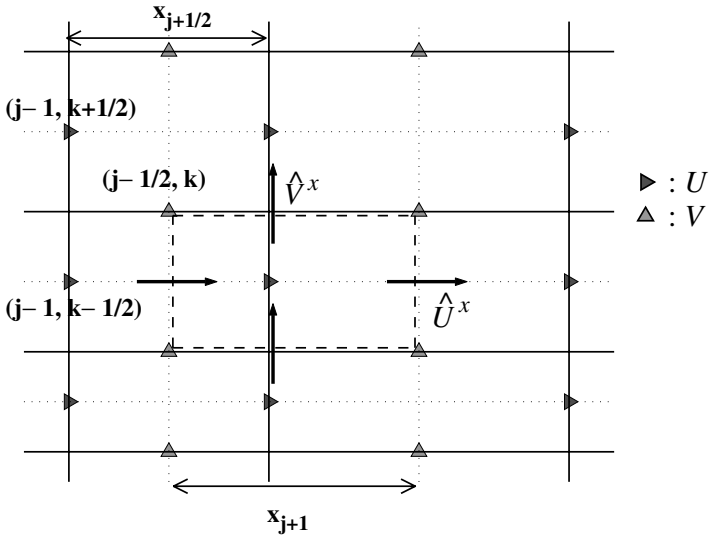

Fig. 4. A control volume for a U-velocity location and inward/outward fluxes using the area-weighted convective velocity, on a two-dimensional staggered grid.

Reference to Fig. 4 shows that in the x-direction, the V-velocity is stored at $x_{j+\frac{1}{2}}$. At x_j it must be found via interpolation – either volume averaging, arithmetic mean, or linear interpolation, denoted by superscript V, A or L. When the U-velocity is needed at $x_{j+\frac{1}{2}}$ it must be interpolated between values at j and $j+1$. We refer to the V as being cell-centered on the x-grid, because it is stored at the $j+\frac{1}{2}$ points, and to U as being vertex centered.

The expressions of the denominator in Eqs. (32) and (10) are different in general, although they are equivalent in a vertex-based grid system. Part of the difficulty in discussing mesh stretch effects is that a staggered grid is rather a mixture of both vertex and cell-centered systems. Hence, in the x-direction, the staggered grid provides a vertex-based formulation for the U equation, but a cell-centered formulation for the V and W equations.

On a vertex-based mesh, the distance between two neighboring nodes $x_{j+1}-x_j=\Delta x_{j+\frac{1}{2}}$ is given by the mesh spacing *directly*. On a cell-centered mesh, however, the distance between nodes is $x_{j+\frac{1}{2}}-x_{j-\frac{1}{2}}=(x_{j+1}-x_{j-1})/2\equiv\Delta x_j$. The volume-weighted average (32) should adopt the sum of interpolation weights, $\Delta x_{j+\frac{1}{2}}+\Delta x_{j-\frac{1}{2}}$, as its denominator. Instead, we employ $2(x_{j+\frac{1}{2}}-x_{j-\frac{1}{2}})$, so that this average is consistent with global conservation. When applied to interpolate a value at $j+\frac{1}{2}$ the denominator becomes

$$2(x_{j+1}-x_j)\neq\Delta x_{j+1}+\Delta x_j.$$

Hence, Eq. (32) can be considered to be a *modified* volume-weighted average. If Eq. (32) is used on a cell-centered mesh, the discrepancy causes an additional error term in a first-order derivative that is $O(h\cdot \mathrm{d}^2h/\mathrm{d}x^2)$, where h denotes mesh width. However, our numerical experiments have confirmed that this error does not significantly affect the solution compared to the mesh stretch error that is of the order of $h\cdot \mathrm{d}h/\mathrm{d}x$.

Using the area-weighted average defined in Eq. (31), mass conservation in the control volume for the U-velocity can be expressed as the volume-weighted average of the two adjoining cells as follows:

$$\overline{(\mathrm{Cont.})}^{\mathrm{V},x}=\frac{\delta\widehat{U}^x}{\delta x}+\frac{\delta\widehat{V}^x}{\delta y}.$$

Note that the volume average is applied to the discrete derivatives, not to the variables, U and V themselves. The right side follows because of Eq. (32).

As will be shown later, the definition (31) must be adopted for convective velocity, or flux velocity, in order to retain the mathematical equivalence between the divergence form and the advective form. A schematic view of a finite volume formulation on a non-uniform mesh, using an area-weighted convective velocity ($\hat{V}$) is shown in Fig. 4.

3.3. The proposed schemes on non-uniform mesh

Using the interpolation operators of Eq. (32) and Eqs. (9) and (10), we formulate the following three convective schemes on non-uniform mesh which are analogous to FD-1–3 (see [3] for further details).

3.3.1. Scheme I

The application of area-weighted average to flux velocity and arithmetic mean to momentum velocity leads to kinetic energy conservation; an equivalent advective form can be formulated by employing volume-weighted averages. The resulting convective scheme, denoted *Scheme I*, can be written in divergence and advective forms for the U-velocity as follows:

$$\frac{\partial UU}{\partial x}+\frac{\partial VU}{\partial y}\approx(\mathrm{Div.\text{-}I})_x\equiv\frac{\delta(\widehat{U}^x\overline{U}^{\mathrm{A},x})}{\delta x}+\frac{\delta(\widehat{V}^x\overline{U}^{\mathrm{A},y})}{\delta y},\tag{33}$$

$$U\frac{\partial U}{\partial x}+V\frac{\partial U}{\partial y}\approx(\text{Adv.-I})_x\equiv\overline{\widehat{U}^x\frac{\delta U}{\delta x}}^{\mathrm{V},x}+\overline{\widehat{V}^x\frac{\delta U}{\delta y}}^{\mathrm{V},y}. \tag{34}$$

$(\text{Adv.-I})_x$ is connected with $(\text{Div.-I})_x$ via

$$(\text{Adv.-I})_x=(\text{Div.-I})_x-U\cdot\overline{(\text{Cont.})}^{\mathrm{V},x}. \tag{35}$$

These formulas are similar to those of Morinishi et al. [6], but have been extended to a non-uniform grid system.

The conservation of kinetic energy is derived as

$$U\cdot(\text{Div.-I})_x-\frac{U^2}{2}\cdot\overline{(\text{Cont.})}^{\mathrm{V},x}=\frac{1}{2}\left[\frac{\delta(\widehat{U}^x\widetilde{UU}^x)}{\delta x}+\frac{\delta(\widehat{V}^x\widetilde{UU}^y)}{\delta y}\right], \tag{36}$$

where the operator $\sim^x$ interpolates a product in the x-direction [6]

$$\widetilde{\phi\psi}^x\Big|_{j+\frac{1}{2}}=\frac{1}{2}\phi(x_{j+1})\psi(x_j)+\frac{1}{2}\phi(x_j)\psi(x_{j+1}). \tag{37}$$

Since (Div.-I) is conservative for momentum by its definition, these schemes locally conserve both momentum and kinetic energy if the continuity equation is satisfied. This form often is preferred, as the globally conserved properties, especially energy, may stabilize the entire field.

However, often accuracy is of more concern than conservation. Thus, alternative forms warrant consideration. The interpolations used in Eqs. (33) and (34) increase the lowest-order truncation errors, thereby degrading accuracy.

3.3.2. Scheme II

By applying linear interpolation to evaluate the inter-cell flux, we obtain the following divergence form:

$$(\text{Div.-II})_x\equiv\frac{\delta(\widehat{U}^x\overline{U}^{\mathrm{L},x})}{\delta x}+\frac{\delta(\widehat{V}^x\overline{U}^{\mathrm{L},y})}{\delta y}. \tag{38}$$

This is denoted *Scheme II*. This inter-cell flux form is conservative for momentum, but not for kinetic energy in the presence of non-uniform mesh spacing.

The natural linear interpolation is equivalent to arithmetic mean in the vertex grid direction. Thus

$$\overline{U}^{\mathrm{L},x}(j+1/2)=\frac{1}{2}(U_{j+1}+U_j)=\overline{U}^{\mathrm{A},x};$$

similarly $\overline{V}^{\mathrm{L},y}=\overline{V}^{\mathrm{A},y}$.

The corresponding advective form is

$$(\text{Adv.-II})_x\equiv\overline{\widehat{U}^x\frac{\delta U}{\delta x}}^{\mathrm{V},x}+\overline{\widehat{V}^x\frac{\delta U}{\delta y}}^{\mathrm{A},y}=(\text{Div.-II})_x-U\cdot\overline{(\text{Cont.})}^{\mathrm{V},x}. \tag{39}$$

Compared to $(\text{Adv.-I})_x$, Eq. (34), the advective form of Scheme II employs an arithmetic average in the vertex-based directions, or for the $\partial/\partial y$ term, instead of a volume-weighted average. This reduces the lowest-order mesh stretch error in the y-direction. In the V equation $(\text{Adv.-II})_y$, an arithmetic mean is applied to $\partial/\partial x$.

3.3.3. Scheme III

Another scheme of interest can be constructed by removing the second-order diffusion error of mesh stretch. Utilizing a linear interpolation operator in the advective form for both the x and y-directions, we have

$$(\text{Adv.-III})_x \equiv \overline{\widehat{U}^x \frac{\delta U}{\delta x}}^{\mathrm{L},x} + \overline{\widehat{V}^x \frac{\delta U}{\delta y}}^{\mathrm{L},y}, \tag{40}$$

which is denoted *Scheme III*. In this scheme, second-order accuracy is enforced by applying linear interpolation to an advective form. The corresponding conservative divergence form does not exist. However, we could define (Div.-III) as follows:

$$(\text{Div.-III})_x \equiv (\text{Adv.-III})_x + U \cdot \overline{(\text{Cont.})}^{\mathrm{V},x}. \tag{41}$$

This divergence form is not conservative; therefore Eq. (41) does not conserve momentum or kinetic energy exactly with variable mesh spacing, even if continuity is enforced.

4. Numerical tests

Fully turbulent flow in a uniform plane channel was simulated on a mesh with stretching in the streamwise direction, as well as in the wall-normal direction. The channel size is $(8H, 2H, 2.4H)$, where H is the half channel height, in the streamwise, wall-normal, and spanwise directions, respectively. The grid size is $128 \times 80 \times 32$. In both the streamwise and spanwise directions, periodic boundary conditions are imposed. A constant pressure drop is applied between the inlet and outlet of the channel. The resulting Reynolds number, Re, based on H and the maximum mean velocity $U_{\max}$, is about 4000, while Re_τ based on H and the friction velocity u_τ is 250.

The dissipation term in the $\overline{v^2}$ budget, ε_{22}, is chosen as a parameter to compare the relative accuracy of the three schemes. The terms of the $\overline{v^2}$ budget are relatively small and are sensitive to numerical inaccuracies. In the streamwise direction, the mesh spacing is distributed symmetrically about $x = 4H$. The mesh contracts in $x < 4H$, and expands in $x > 4H$. The ratio of mesh stretch diffusion to molecular viscosity, $U_{\max}\delta(\Delta x)/\nu$, ranges approximately from -20 to 20. This can be called the mesh stretch Reynolds number. It is relatively large, to illustrate the nature of mesh stretch error. Smaller values will reduce the size of error, but it remains present in well resolved simulations [3].

In addition to the three schemes discussed previously, the following scheme in a divergence form is also tested here:

$$(\text{Div.-Orig.})_x \equiv \frac{\delta(\overline{U}^{\mathrm{L},x}\overline{U}^{\mathrm{L},x})}{\delta x} + \frac{\delta(\overline{V}^{\mathrm{L},x}\overline{U}^{\mathrm{L},y})}{\delta y}. \tag{42}$$

Instead of the area-weighted average to evaluate the mass flux velocity at the inter-cell face, rather intuitively, linear interpolation weights are adopted. Eq. (42) has been used in previous DNS and LES studies, although without a strong mesh stretch in the streamwise direction. While Eq. (42) may improve the accuracy in the cell-based directions (the y- and z-directions for the U equation) it does not in the other direction. Moreover, it gives up the connection to an equivalent advective form, which leaves the error estimate unclear. We include it simply for a connection to common practice.

Fig. 5 shows the distributions of $\varepsilon_{22}^+ \equiv \nu\varepsilon_{22}/u_\tau^4$ in the y-direction. The mesh plot is of the two-dimensional distribution $\varepsilon_{22}(x, y)$ for (Div.-II). Each vertical line of the mesh indicates an x grid location, whereas each curve drawn in the x-direction corresponds to an ε_{22}-distribution at a particular y grid location. The maximum ε_{22} for a given x location occurs approximately at $y = 0.2H$. The other line plots show the maximum values for each x location. Ideally, these profiles should be straight lines, independent of x, because the channel is uniform.

Among the four convective forms, (Div.-Orig) and (Div.-I) show the largest over-shoot errors, slightly downstream of $x = 4H$. In the mesh-contracting region, $x < 4H$, ε_{22} gradually decreases, and then rises

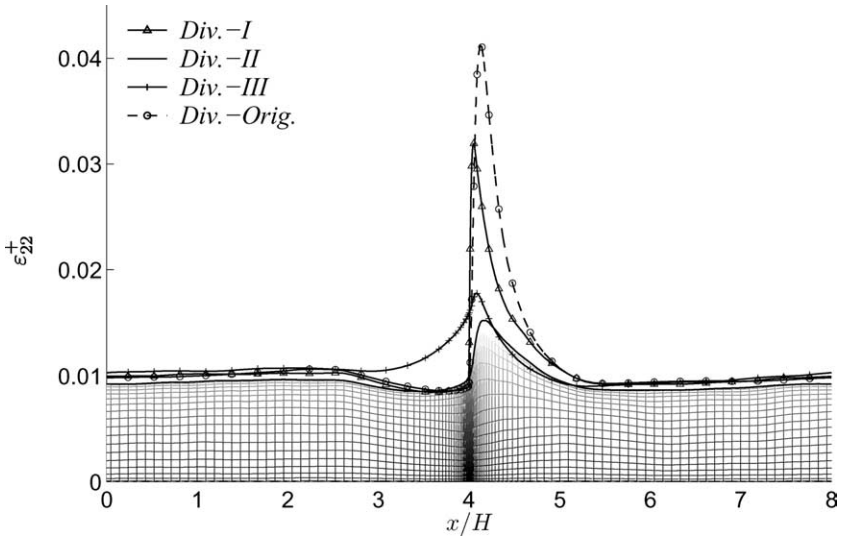

Fig. 5. Comparison of ε^+_{22} over/under-shoot due to the mesh stretch error. The mesh plot shows $\varepsilon^+_{22}(x,y)$ for (Div.-II).

sharply in the mesh-stretching region, $x > 4H$. This agrees with the first excess, then negative diffusion added by the mesh stretch in each region. The same tendency is observed for (Div.-II), although the over-shoot error is smaller.

(Div.-III) shows a nearly symmetric profile on $x = 4H$. It would not produce either excess diffusion or anti-diffusion based on a Taylor series analysis (corresponding to $k_n \to 0$ in FD-3 in Fig. 1). Nevertheless a considerable over-shoot is observed near the middle of the channel. This demonstrates the need to analyze the shorter wavelength error by Fourier analysis. As seen in Fig. 1, (Div.-III) produces a significant diffusive error at large k_n: the error is an anti-diffusion in a mesh-contracting region, and positive-diffusion in a mesh-stretching region. This corresponds to the observation in Fig. 5; ε_{22} increases as the mesh spacing decreases in $x < 4H$ due to anti-diffusion, and decreases in $x > 4H$.

In addition to the extra/anti-diffusive error, the two-dimensional (Div.-I) form has a first-order derivative error of $O(h \cdot h'')$, in the y-direction for U, and in the x-direction for V. For the grid of the present study, a considerable magnitude of that error occurs at only a few node points around $x = 4H$, where the slope of the Δx distribution changes discontinuously. The maximum error of convective velocity is about 4% at $x = 4H$, whereas the error is less than 0.5%, everywhere else. This first-order derivative error is removed in the other schemes.

The mesh stretching affects not only the $\overline{v^2}$ budget, but also $\overline{v^2}$ itself. Fig. 6 shows the $\overline{v^2}$ fluctuations from the streamwise average for the schemes examined in the channel flow simulation. The presented profiles are at $y = 0.16H$, where the over-shoot error of ε_{22} reaches its maximum. Due to a short sampling time, these data still exhibit statistical fluctuations, approximately $\pm 3\%$ of $\overline{v^2}$. However, the under-shoot in the mesh-contracting region, $x < 4H$, and the over-shoot in the mesh-expanding region, $x > 4H$, which can be estimated as $\pm 13\%$ for (Div.-I), are statistically significant. The (Div.-II) scheme shows the same tendency as (Div.-I) and (Div.-Orig.), but the range of fluctuation is about halved. (Div.-III) presents the opposite effect on the sign of mesh stretch ratio, compared to the other schemes, as also seen in the ε_{22} profiles.

Although Figs. 5 and 6 show the particular difference between (Div.-II) and (Div.-III), and the over-shoot of (Div.-II) is slightly smaller than that of (Div.-III), we cannot ascertain which is better suited to DNS with mesh stretch. However, a more detailed DNS test on these two schemes shows that the (Div.-III)

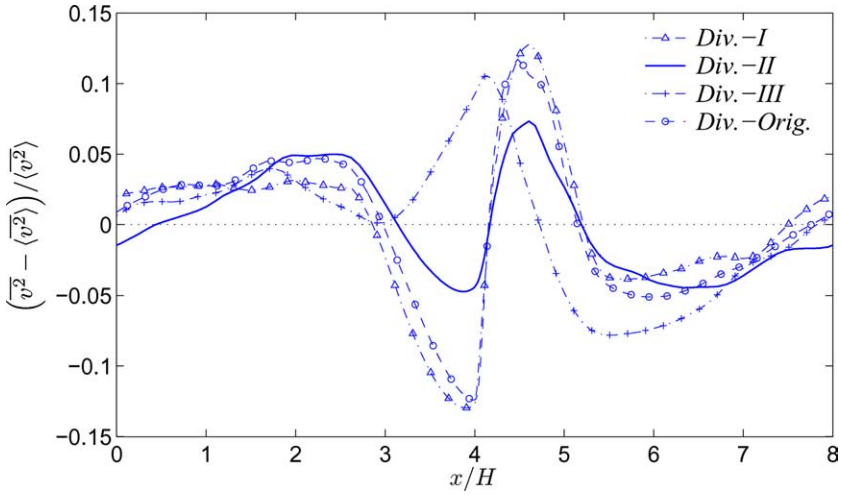

Fig. 6. Deviation of $\overline{v^2}$ from its streamwise average $\langle\overline{v^2}\rangle$ at $y = 0.16H$.

form retains a certain level of error in statistics even if the mesh stretch ratio is reduced. The main reason is that this form, Scheme III, becomes fairly diffusive in high-wavenumber Fourier modes, as seen in the linear test case. As statistics are sampled, it accumulates erroneous behavior caused by high-frequency modes in full turbulence simulations, even though Scheme III shows the best performance in the simple convection problem, at low wavenumbers. Also, it may be added that this formulation conserves neither kinetic energy or momentum, when mass conservation is enforced.

5. Conclusion

Mesh stretch effects on conservation properties and accuracy of numerical forms of convection terms were reviewed and discussed for second-order, centered difference schemes. It was confirmed that to avoid spurious errors, consistency between mass and momentum equations is essential in constructing a proper form of conservative schemes on a non-uniform mesh.

However, mesh stretching locally causes significant diffusive effects on an anti-symmetric, centered difference scheme. It has been verified that either anti- or positive-diffusion is produced, depending on the sign of mesh stretch ratio and convection velocity. In turbulence simulations, however, higher-order truncation errors also have a significant effect on high wavenumber modes, or small eddies in the dissipative range. Straightforward treatment of convective schemes to eliminate the lowest-order truncation error may not improve statistical results, as was seen in Scheme III.

Overall, Scheme II, which was suggested in Eq. (38), has been shown to minimize the errors in statistical data, relative to other centered difference schemes with three-point stencils. It does not conserve quadratic quantities but the momentum equations can still be written in a conservative form. It employs area-weighted averages to formulate inter-cell flux velocity, and linear interpolations to evaluate other quantities. This is equivalent to an arithmetic mean of finite difference terms at two adjoining inter-cell faces in a cell-centered grid system. This simple change from the kinetic energy conservation form, Scheme I, significantly reduces the mesh stretch error on statistics, especially on the dissipation terms in Reynolds stress budgets. An application of this method to DNS of a ribbed channel is contained in [3].

Acknowledgements

This work was sponsored by the Office of Naval Research, grant number N00014-01-1-0419-P00003.

References

[1] K. Bryan, A scheme for numerical integration of the equations of motion of an irregular grid free of non-linear instability, Monthly Weather Review 94 (1966) 39–40.
[2] J.H. Ferziger, M. Peric, Computational Methods for Fluid Dynamics, second ed., Springer Verlag, Berlin, 1999.
[3] T. Ikeda, P.A. Durbin, Direct Simulations of a Rough Wall Channel Flow, Stanford University, Mechanical Engineering report TF-81, 2002.
[4] A.G. Kravchenko, P. Moin, On the effect of numerical errors in large eddy simulations of turbulent flows, Journal of Computational Physics 131 (2) (1997) 310–322.
[5] D.K. Lilly, On the computational stability of numerical solutions of time dependent non-linear geophysical fluid dynamics problems, Monthly Weather Review 93 (1965) 11–26.
[6] Y. Morinishi, T.S. Lund, O.V. Vasilyev, P. Moin, Fully conservative higher order finite difference schemes for incompressible flow, Journal of Computational Physics 143 (1998) 90–124.
[7] S.A. Piacsek, G.P. Williams, Conservation properties of convection difference schemes, Journal of Computational Physics 6 (1970) 392–405.
[8] P.R. Spalart, Hybrid RKW3 + Crank–Nicolson scheme, Internal report, NASA-Ames Research Center, Moffett Field, CA, 1987.